A Decentralized Model Predictive Control Approach to Power Management of a Fuel Cell-Ultracapacitor Hybrid

Ardalan Vahidi Wesley Greenwell
Department of Mechanical Engineering, Clemson University

Abstract— **This paper presents an application of decentralized model predictive control (MPC) to a fuel cell-ultracapacitor hybrid. Dedicated subsystem level MPC controllers are developed that control a fuel cell and an ultracapacitor current and enforce point-wise-in-time constraints of each subsystem independently of each other. A simple supervisory scheme determines the power split between the fuel cell and the ultracapacitor. Nonlinear simulations show that the decentralized control design is successful in enforcing subsystem level constraints while achieving system-level power demand. The proposed decentralized approach has practical advantages over a centralized MPC design because of its potential to decrease online computations and more importantly because of its compatibility with a modular software/hardware architecture.**

I. Introduction

Power management of hybrid electric vehicles, including fuel cell hybrids, requires a well-designed control strategy to ensure best use of multiple power sources at the system level while conforming to the requirements and limitations of the subsystem level components. To meet the system and subsystem level (possibly conflicting) requirements, the traditional powertrain control approach is mostly logic-based with a large set of logical checks, pre-calculated tables, and simple control loops. Most power management strategies run based on the instantaneous state of the system and are not predictive in nature. Recent research and practice utilizes more advanced control and optimization techniques to maximize the efficiency of the power management scheme while allowing a systematic control design. Dynamic programming [1], unconstrained optimal control [2] and model predictive control (MPC) [3] methods have been proposed in the past few years for off-line or even real-time solution of the power management problem. In [3], the first author and his colleagues have shown the benefits attainable by a centralized MPC design in power management of a mild fuel cell hybrid which uses an ultracapacitor module during power transients.

In theory, a centralized model predictive control scheme could provide a systematic solution to the increasing complexity of a hybrid electric powertrain with several mechanical and electrical components. However, there are practical limitations to such a centralized MPC design; in particular: 1) The size of the optimization problem can easily exceed the real-time computational capability of current automotive micro-controllers 2) The model-based nature of MPC requires re-tuning of the whole power management scheme if any of the subsystem level components is modified. In other words a centralized controller will not lend itself to a modular software/hardware system architecture.

More recently use of decentralized or distributed MPC has been proposed for controlling large-scale systems such as distributed power grids [4] and control of unmanned air vehicles [5]. The idea in a decentralized MPC approach is to break a large-scale optimization problem into smaller size optimizations, each handled by a dedicated MPC controller. Recent results show that even when the subsystems are coupled in their optimization objective function and constraints, the decentralized approach can generate solutions which are close to the optimal solution obtained by a centralized MPC scheme [4]. Stability of some decentralized MPC algorithms has been recently studied in [6], [7].

Decentralization can be an enabler for modular software and hardware architectures and a hierarchical control design which may be suitable in power management of hybrid electric vehicles. The control computation task can be effectively distributed among multiple processors which communicate with each other through the vehicle control area network (CAN). The purpose of this paper is to demonstrate a simple decentralized MPC design and its performance in power management of hybrid electric vehicles. We have chosen the fuel cell-ultracapacitor power management problem discussed by the first author and his colleagues in [3] as both a challenging and an interesting control problem.

The power response of the 75kW PEM fuel cell system discussed in [3] was limited during power transients due to surge and choke limits of its centrifugal compressor and also a long inlet manifold which slowed supply of air to the cathode. It was shown in [3] that a small ultracapacitor module could be used as a buffer during load transients. Because of the pointwise-in-time constraints that the fuel cell faced and also the need to limit voltage variations of the ultracapacitor module, a centralized MPC design was proposed and was tested successfully in nonlinear simulations of the hybrid system.

In this paper, we evaluate a decentralized MPC design, one in which the fuel cell and ultracapacitor each have its own MPC controller. Figure 1 provides a schematic of the proposed decentralized design as compared to a centralized MPC. Each controller determines the constraint-admissible and optimum value of current that can be taken from the fuel cell or ultracapacitor at each instant in time. While the dynamics and constraints of the fuel cell and the ultracapacitor are decoupled, the controllers are coupled through their

A. Vahidi (corresponding author) is with the Department of Mechanical Engineering, Clemson University, Clemson, SC 29634-0921, E-mail: avahidi@clemson.edu.

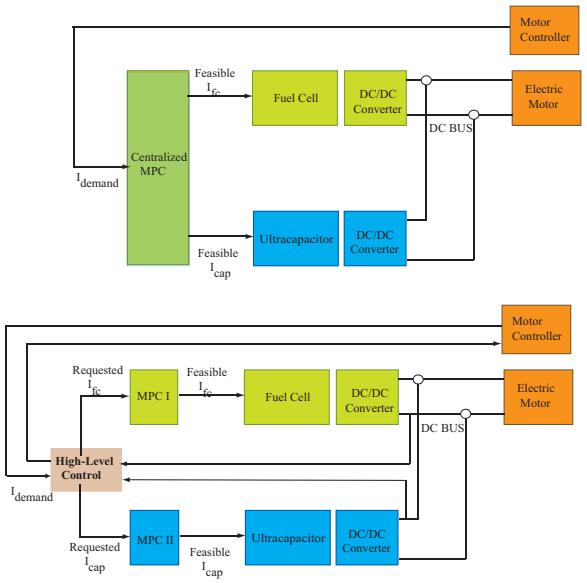

Fig. 1. Decentralized and centralized MPC architectures in a hybrid fuel cell powertrain.

objective functions and the fact that together they should match the power demand. We evaluate the performance of the overall system with decentralized MPC based on nonlinear simulations. Compared to the centralized MPC approach presented in [3], the proposed decentralized approach may have practical advantages because of its potential to decrease online computations and more importantly because of its compatibility with a modular software/hardware architecture.

In the work presented here, we assume that the ultracapacitor module is connected to the BUS through a bi-directional dc/dc converter which extends the range of operation of ultracapacitors beyond what was shown in [3] and ensures a constant BUS voltage. Moreover inclusion of the internal resistance of the ultracapacitor module and a brief discussion of the lower-level power electronics addresses some of the practical issues in implementing such an algorithm.

Section II summarizes the fuel cell system model previously obtained in [8] and more recently discussed in [3], [9] and also outlines the design of an MPC scheme for the stand-alone fuel cell. In section III, a model of the ultracapacitor interfaced to the BUS through a dc/dc converter is presented and MPC-based power management of the ultracapacitor is explained. Section IV is on integration of the closed-loop fuel cell and ultracapacitor systems and demonstrates the performance of decentralized MPC in nonlinear simulations. Section V presents the conclusions.

II. The Fuel Cell System and Its MPC Controller

A schematic of a PEM fuel cell system is shown in Fig. 2. Hydrogen is supplied from a hydrogen tank and its flow is directly controlled by an inlet valve. A compressor supplies high pressure air to the cathode. A control input to the system is the compressor command v_{cm}, which influences the speed of the compressor and consequently the amount of

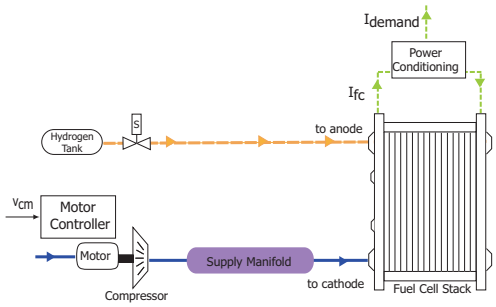

Fig. 2. Schematic of air supply control system

air that is supplied to the cathode. The current taken from the fuel cell I_{fc} can also be controlled through the power electronics, and determines the rate at which hydrogen and oxygen are consumed. Given the current taken from the fuel cell I_{fc}, and the voltage supplied to the compressor motor v_{cm}, (and also the ambient conditions), the state of species in the stack can be determined. In this paper we will keep track of the compressor flow W_{cp} and the pressure downstream of the compressor p_{sm} since they together indicate if the compressor is near choke saturation or surge instability as shown in Fig. 3. The dashed lines shown in this compressor map represent boundaries beyond which compressor surge and choke can occur. Figure 3 shows the evolution of the compressor flow and pressure ratio in the compressor map during the transients of Fig. 4. In this open-loop simulation the 9-state nonlinear fuel cell model described in [8] is used and the compressor command v_{cm} is simply determined as an increasing linear function of current. During a step-up in v_{cm} command, the compressor flow increases faster than the pressure p_{sm} downstream the compressor. As a result the compressor operates near the choke boundary. During a step-down in v_{cm}, the operating trajectory nears the surge boundary. Larger steps in current require larger compressor commands that if applied instantaneously may result in surge or choke. Therefore we would like to enforce pointwise-in-time constraints in the control design to ensure operation of the compressor inside the bounded region and away from the surge and choke regions. Figure 4 also shows a variable called oxygen excess ratio λ_{O_2}, which is defined as the ratio between oxygen supplied and the oxygen reacted in the cathode. Low values of λ_{O_2} may indicate low oxygen concentration in the cathode (oxygen starvation) which could negatively affect the fuel cell voltage response and even permanently damage the cells. To prevent such a condition, we enforce a lower bound on oxygen excess ratio as well.

The 9-state fuel cell model used in the simulation above represents the anode, cathode and return manifold dynamics in addition to the compressor and inlet manifold dynamics. While these subsystems interact, the compressor and oxygen flow dynamics might still be approximated well by a lower order model. A reduced model of the 9-state fuel cell system is obtained in [10] for simulation of the air supply side. The reduced model has only four dynamic states: partial oxygen pressure inside the cathode p_{O_2}, partial nitrogen pressure

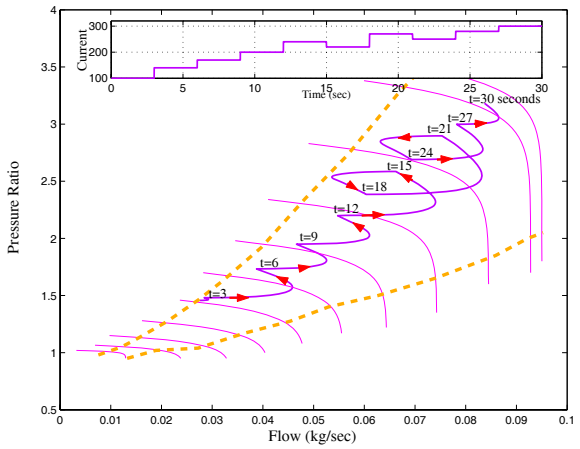

Fig. 3. The compressor response to step changes in current demand.

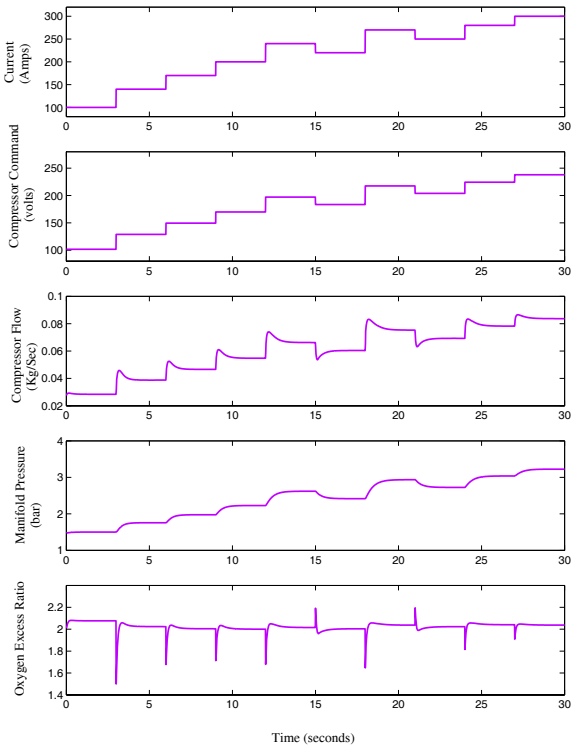

Fig. 4. The fuel cell model response to step changes in current demand.

inside the cathode p_{N_2}, compressor motor speed ω_{cp} and the supply manifold pressure p_{sm}. We use this model in the remainder of this paper. Due to the complexity of the model all the governing equations cannot be easily shown in a concise closed-form. However the general state-space form is:

$$\begin{aligned} \dot{x}_{nl} &= h(x_{nl}, v_{cm}, I_{fc}) \\ y_{nl} &= g(x_{nl}, v_{cm}, I_{fc}), \end{aligned} \tag{1}$$

where the dynamic state vector of the nonlinear system is:

$$x_{nl} = [p_{O_2} \;\; p_{N_2} \;\; \omega_{cp} \;\; p_{sm}]^T,$$

and the outputs of our interest in this paper are

$$y_{nl} = [\lambda_{O_2} \quad W_{cp} \quad p_{sm} \quad V_{fc} \quad P_{cp} \quad I_{fc}^{bus}]^T$$

representing, respectively, oxygen excess ratio λ_{O_2}, compressor air flow W_{cp}, manifold pressure p_{sm}, fuel cell stack voltage V_{fc}, a normalized variable denoting compressor power consumption P_{cp} and the fuel cell current delivered to the BUS I_{fc}^{bus}. Note that using conservation of energy we have $\eta_1 I_{fc} V_{fc} = I_{fc}^{bus} V_{bus}$ where η_1 is the DC converter efficiency.

We will design an MPC controller for the fuel cell which imposes constraints to prevent compressor surge and choke, oxygen starvation and low fuel cell stack voltage, minimize the compressor power usage while tracking a current request from the fuel cell as closely as possible. For control design, the nonlinear fuel cell model is linearized at a representative operating point. We choose the nominal stack current at $I_{fc}^o = 192$ A. The nominal value for oxygen excess ratio is selected at $\lambda_{O_2}^o = 2.0$, which provides maximum fuel cell net power for the nominal current [8]. The compressor motor voltage needed, to supply the optimum air flow that corresponds to I_{fc}^o and $\lambda_{O_2}^o = 2.0$, is $v_{cm}^o = 164$ volts. In the resulting linearized state-space equation there is a direct injection of the input I_{fc} in the output equation. To cast the state-space model in the standard MPC format with no direct injection of input to output, we augment a fast first-order linear filter to the system which results in a linearized model with 5 states and 6 outputs. Furthermore for asymptotic rejection of output disturbances by the controller, a step disturbance model and a disturbance observer is augmented to the system. The details are omitted here in the interest of space. A similar process is explained in more detail in [3]. Interested reader can find more in depth discussion of disturbance models for MPC in [11], [12].

The MPC problem can be formulated by first defining a performance index that penalizes 1) the deviations of the fuel cell current delivered to the BUS I_{fc}^{bus} from the requested current at the BUS from the fuel cell $I_{fc,req}^{bus}$ 2) compressor power use P_{cp} 3) deviations from the desired oxygen excess ratio of 2.0 4) the rate of change of fuel cell current:

$$\begin{aligned} J = \sum_{j=1}^{P} & (\|I_{fc,req}^{bus}(k+j) - I_{fc}^{bus}(k+j|k)\|_{r_1(j)}^2 + \\ & \|P_{cp}(k+j|k)\|_{r_2(j)}^2 + \|\lambda_{O_2}(k+j|k) - 2.0\|_{r_3(j)}^2 + \\ & \|\Delta I_{fc}(k+j-1)\|_{r_4(j)}^2) \end{aligned} \tag{2}$$

Here $k+j|k$ denotes the prediction at instant k for instant $k+j$ and P is the length of the prediction horizon. The scalars $r_i(j)$ $i = 1,2,3,4$ are the penalty weights at step j; in other words time-varying penalty weights may be chosen if needed. The control horizon is in general $N \leq P$. Since the future current request is not known, we assume that the current request over a prediction horizon is equal to the current demand in the beginning of the optimization window:

$$I_{fc,req}^{bus}(k+j) = I_{fc,req}^{bus}(k)$$

At each instant k, N future current values

$$[I_{fc}^{bus}(k+1) \;\; I_{fc}^{bus}(k+2) \;\; \ldots \;\; I_{fc}^{bus}(k+N)]$$

are sought that minimize the above performance index subject to the linear state-space equations of the fuel cell system

(augmented with the disturbance model) and the following inequality constraints enforced $\forall j = 1, 2, ..., P$:

- The nonlinear surge and choke boundaries shown in Fig. 3 can be approximated by straight lines for most part of the operating region. The constraints can then be represented by two linear inequalities and as a function of compressor flow and supply manifold pressure:

$$\begin{aligned} -0.0506\delta W_{cp} + \delta p_{sm} &\leq 0.4, \\ 0.0155\delta W_{cp} - \delta p_{sm} &\leq 0.73. \end{aligned} \tag{3}$$

  where the operator δ indicates the deviation of the variables from their operating conditions.
- The lower limit on oxygen excess ratio is set to 1.9 to avoid large drops in the cathode oxygen partial pressure and hence prevent stack oxygen starvation. Also an upper bound of 2.5 is imposed to prevent large oxygen pressure at the cathode[1]:

$$1.9 \leq \lambda_{O_2} \leq 2.5 \tag{4}$$

- Bounds on the fuel cell voltage are needed in accordance with the requirements of the dc/dc converter. Here we impose the following bounds:

$$200 \leq V_{fc} \leq 300 \tag{5}$$

The above constrained optimization problem is solved in a receding horizon fashion. The solution determines the feasible and optimal current that can be delivered by the fuel cell at each instant. Our assumption is that once the optimum value of current is determined by the MPC scheme, the delivery can be facilitated by the lower level converter controller. The converter dynamics is typically much faster than power dynamics of the fuel cell and therefore is not considered here.

We have designed and tested the MPC controller for the fuel cell by running simulations on the nonlinear fuel cell model described above. After several iterations, we chose the horizons $P = N = 5$ and the control weights $r = [0.5\ 1\ 1\ 0.1]$ for all values of j. Figures 5 and 6 summarize the simulation results of the nonlinear fuel cell closed-loop system during step changes in current demand. The fuel cell follows the current demand as closely as possible; voltage and compressor surge and choke constraints are met at all times, the oxygen starvation constraint is also met almost always except at two instances when small excursions occur due to infeasibility of the constraints.

III. The Ultracapacitor and its MPC Controller

A fuel cell system buffered with a small ultracapacitor module will have better load following capability than a stand-alone fuel cell. High power density of ultracapacitors which is an order of magnitude higher than batteries [13] and the capability to deliver currents instantaneously, make ultracapacitors an excellent power boost device.

[1]These bounds are design variables selected to reduce the risk of oxygen pressure fluctuations; other bounds or provisions may be used in different setups.

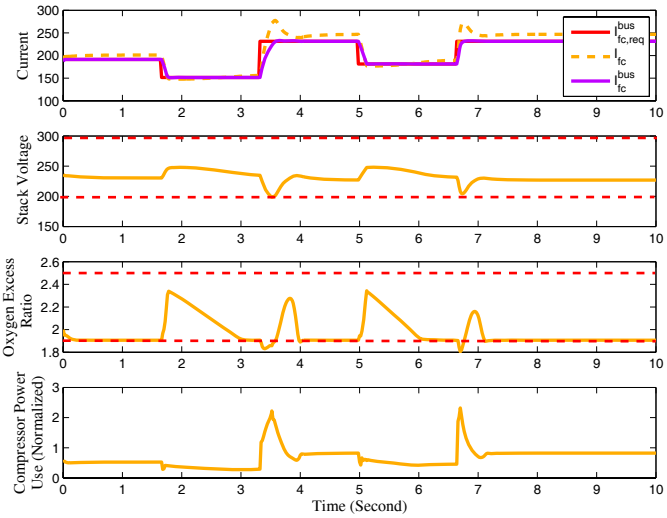

Fig. 5. Fuel cell response to step-changes in current demand. The horizontal dashed lines represent the constraints.

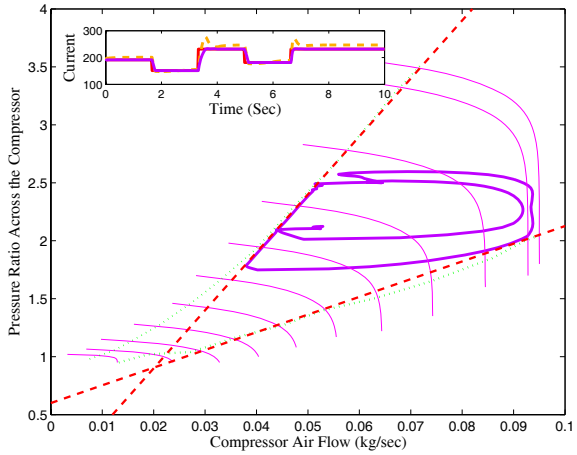

Fig. 6. Compressor map shows both surge and choke constraints are enforced during the variations in the fuel cell current shown in the insert plot.

The stored charge in an ultracapacitor is characterized by a normalized measure called the state of charge, $SOC \in [0, 1]$. The state of charge of 0 represents no stored charge and 1 corresponds to full charge. The rate of change in ultracapacitor state of charge is proportional to the discharging or charging current I_{cap} (positive or negative values of current denote discharging or charging respectively):

$$\frac{d}{dt} SOC(t) = \frac{-1}{CV_{max}} I_{cap}(t) \tag{6}$$

where C is the capacitance of the ultracapacitor module in Farads and V_{max} is its voltage at full charge. In our design we assume the maximum voltage of $V_{max} = 360$ volts. We choose the capacitance to be 0.65 Farads which is a sufficiently large power buffer during fuel cell load transients. One possible configuration that realizes this value of capacitance, is a bank of 120 ultracapacitors, each with capacitance of 80 Farads and a rated voltage of 3 volts, connected in series. Together the package of ultracapacitors can provide

a maximum voltage of 360 volts and a storage capacity of 11 Watt-hours. This size of ultracapacitors can shield the fuel cell from starvation or prevent compressor surge. Note here that larger capacitances will be potentially needed for start-up or other power requirements.[2]

The net voltage generated by the ultracapacitor is a function of ultracapacitor state of charge and the voltage lost to internal resistance of the ultracapacitor module and the connecting cables:

$$V_{cap}(t) = SOC(t)V_{max} - RI_{cap}(t) \tag{7}$$

where R denotes the lumped resistance of ultracapacitor module and cables. The ultracapacitor dynamics is represented by the first-order ordinary differential equation (6) in which the input is I_{cap} and the single states is SOC. The outputs of interest are $y_{cap} = [SOC, \quad V_{cap}, \quad I_{cap}]$. The system is is linear in both the state and output equations. The system is discretized with sampling time of T_s. Similar to what was described in the previous section for the fuel cell, a fast first order filter is augmented to avoid direct injection of input in the output equation. Also a step disturbance model and an observer are augmented to the system. The details are omitted here in the interest of space.

In our proposed architecture, the ultracapacitor is connected to the BUS via a bi-directional dc/dc converter which facilitates active control of charge and discharge of the ultracapacitor[3]. We neglect the dynamics of the dc/dc converter as its dynamics is much faster than ultracapacitor's charge/discharge dynamics; instead we use a static model for the converter. Conservation of energy yields:

$$V_{bus}I_{cap}^{bus} = \eta_2 V_{cap}I_{cap} \tag{8}$$

where I_{cap}^{bus} is the contribution of the ultracapacitor to the BUS current, V_{bus} is the BUS voltage and $0 < \eta_2 < 1$ denotes the converter efficiency during a discharge cycle[4]. Equations (7) and (8) yield:

$$I_{cap}^{bus}(t) = \frac{\eta_2}{V_{bus}} I_{cap}(t)(SOC(t)V_{max} - RI_{cap}(t)) \tag{9}$$

The power request from the ultracapacitor is $P_{cap,req} = V_{bus}I_{cap,req}^{bus}$ in which $I_{cap,req}^{bus}$ is the current request from the ultracapacitor on the BUS downstream the converter. Equivalently we can formulate the problem in terms of $I_{cap,req}$ which is the required capacitor current upstream of the dc/dc converter[5]. By writing the balance of energy across the dc/dc converter we obtain:

$$P_{cap,req} = \eta_2 I_{cap,req}(t)\,(SOC(t)V_{max} - RI_{cap,req}(t)) \tag{10}$$

Solving the resulting quadratic equation, we find:

$$I_{cap,req}^{1,2} = \frac{SOCV_{max} \pm \sqrt{(SOCV_{max})^2 - 4RP_{cap,req}/\eta_2}}{2R} \tag{11}$$

For the equation to have solutions, the following condition should hold:

$$(SOC(t)V_{max})^2 - 4RP_{cap,req}(t)/\eta_2 \geq 0$$

$$\Rightarrow P_{cap,req}(t) \leq \eta_2 (SOC(t)V_{max})^2/4R$$

Which imposes an upper limit to the power that can be taken from the ultracapacitor and is a function of ultracapacitor state of charge. The supervisory controller should take this constraint into account when requesting power from the ultracapacitor controller. Moreover, note that equation (11) provides two feasible solutions for I_{cap}^{req}. Both currents satisfy the power request, since the resistive losses are larger for the larger current, the smaller current is selected:

$$I_{cap,req} = \frac{SOCV_{max} - \sqrt{(SOCV_{max})^2 - 4RP_{cap,req}/\eta_2}}{2R} \tag{12}$$

In the proposed decentralized control architecture, a dedicated controller should maintain state of charge and voltage of the ultracapacitor within allowable bounds while delivering the power requested from the ultracapacitor as closely as possible. While rule-based control laws can be devised for active control of the ultracapacitor, multiple explicit hard constraints may be better handled by resorting to a model predictive control strategy. The MPC problem can be formulated by first defining a performance index that penalizes 1) the deviations of the ultracapacitor current from the requested current 2) the deviations of ultracapacitor state-of-charge from its nominal value SOC_0 and 3) the rate of change of ultracapacitor current, over a finite future horizon of length P:

$$J = \sum_{j=1}^{P} (\|I_{cap,req}(k+j) - I_{cap}(k+j|k)\|_{q_1(j)}^2 + \|SOC_0(k+j) - SOC(k+j|k)\|_{q_2(j)}^2 + \|\Delta I_{cap}(k+j-1)\|_{q_3(j)}^2) \tag{13}$$

similar to the fuel cell problem, P is the prediction horizon and $q_i(j)$ $i = 1,2,3$ are the penalty weights at step j. At each instant k, a finite future current sequence

$$[I_{cap}(k+1) \;\; I_{cap}(k+2) \;\; \ldots \;\; I_{cap}(k+N)]$$

is sought that minimizes the above performance index subject to the linear state-space equations of the system (augmented with the disturbance model) and the following inequality constraints enforced $\forall j = 1,2,...,P$:

- Bounds on the ultracapacitor state-of-charge to prevent complete discharge or overcharge of the ultracapacitor module:

$$0.6 \leq SOC(k+j) \leq 0.8$$

[2]In [14], Rodatz et al. have used ultracapacitors in a hybrid fuel cell vehicle to assist the fuel cell during hard accelerations and for storing the energy from regenerative braking. A much larger buffer size is required for their purpose. They have provided this buffer by 282 pair-wise connected capacitors, each with capacitance of 1600 F. The storage capacity is 360 Watt-hours.

[3]Our assumption is that the fuel cell converter maintains the BUS voltage constant.

[4]This equation is valid during a discharge cycle. During a charge cycle we replace this equation by $\eta_3 V_{bus}I_{cap}^{bus} = V_{cap}I_{cap}$ where η_3 is the converter efficiency during a charge cycle.

[5]The ultracapacitor model is nonlinear with $I_{cap,req}^{bus}$ as an output but linear with $I_{cap,req}$ as an output; therefore working with $I_{cap,req}$ simplifies the control design.

- Operational bounds on the dc/dc converter input voltage V_{cap}, specified by the converter manufacturer are also imposed. Here we assume the following bounds:

$$200 \leq V_{cap}(k+j) \leq 300$$

This constrained optimization problem is solved in a receding horizon fashion. The solution determines the feasible and optimal value of current that can be delivered (or accepted) by the ultracapacitor at each instant. Our assumption is that once this optimum current is determined by the MPC scheme, the lower level converter controller can achieve it.

We have designed and tested the MPC controller for the ultracapacitor by running simulations on the ultracapacitor model described above. The nominal state-of-charge was selected at $SOC_0 = 0.7$. After several iterations we chose the horizons $P = N = 20$ and the penalty weights $q_1 = 1, q_3 = 0.1 \ \forall j$. We determined that a fixed "large" penalty weight on the state-of-charge limits utilization of the ultracapacitor, and a fixed "small" weight compromises charge-sustaining. To remedy this problem, a time-varying penalty weight q_2 was selected to penalize deviations from the nominal state-of-charge:

$$q_2(j) = j^2 \quad j = 1, 2, ..., P$$

during each optimization horizon; lower initial weighting allows better utilization of the ultracapacitor while larger terminal weights enforce recharging when a charging power source like a fuel cell is available. Figure 7 shows results of a sample simulation during step changes in current demand. It should be noted that here, in the absence of the fuel cell, the ultracapacitor is not charged back to the nominal state of charge at steady-state. However the constraints imposed on the state-of-charge ensure that the ultracapacitor is always partially charged.

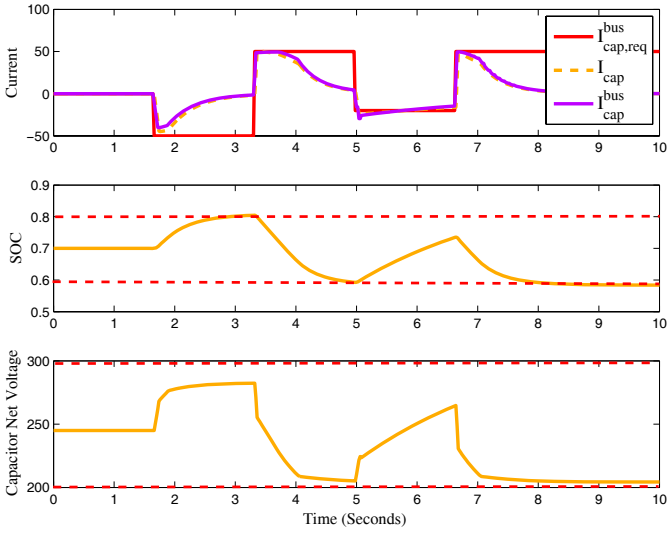

Fig. 7. Ultracapacitor response to step-changes in current demand. The horizontal dashed lines represent the constraints.

IV. Coordination of the Fuel Cell and Ultracapacitor

In this paper we use a simple strategy to determine the current split between the fuel cell and ultracapacitor. We postpone rigorous theoretical investigation of this proposed scheme and its influence on convergence of the decentralized MPC algorithm to a future publication.

The current demand on the ultracapacitor is chosen to be the difference between the total current demand and current delivered to the BUS by the fuel cell:

$$I^{bus}_{cap,req}(k) = I_{demand}(k) - I^{bus}_{fc}(k) \tag{14}$$

Similarly the current demand from the fuel cell is determined by the difference between the current demand and the current delivered to the BUS by the ultracapacitor:

$$I^{bus}_{fc,req}(k) = I_{demand}(k) - I^{bus}_{cap}(k) \tag{15}$$

This formulation couples the cost functions (2) of the fuel cell MPC and (13) of the ultracapacitor MPC. In [4], a number of approaches for solving such optimization problems in a decentralized MPC framework is proposed. In this paper we use the simpler approach which solves the optimization problems independently without iterative communications between the solvers. Future research can build on our proposed approach and 1) use communication between the solvers at each sampling instant and solve the optimization problems iteratively 2) utilize the future control sequence of each MPC as preview information for the other MPC.

Note that summation of both sides of equations (14) and (15) yields:

$$I^{bus}_{cap,req}(k) + I^{bus}_{fc,req}(k) = 2I_{demand}(k) - (I^{bus}_{fc}(k) + I^{bus}_{cap}(k)) \tag{16}$$

Since both MPC controllers have zero steady-state tracking errors when the constraint are inactive, we have:

$$I^{bus}_{fc} \rightarrow I^{bus}_{fc,req}$$
$$I^{bus}_{cap} \rightarrow I^{bus}_{cap,req},$$

at steady-state assuming inactive constraints, therefore from (16):

$$I^{bus}_{fc}(k) + I^{bus}_{cap}(k) \rightarrow I_{demand}$$

We ran a nonlinear simulation with the decentralized MPCs and the power management strategy given by (14) and (15). Figures 8 and 9 show the time history of system and compressor response during step changes in the BUS current demand denoted by δI^{bus}_{demand}. It can be seen that the sum of the currents delivered to the BUS by the fuel cell and the ultracapacitor $\delta I^{bus}_{total} = \delta I^{bus}_{fc} + \delta I^{bus}_{cap}$ matches the current demand. In other words, while the controllers do not communicate the value of their states or objective functions, they are able to collaboratively meet the system level current demand while each enforces the constraints of its own subsystem. Therefore, the decentralized design can match a centralized design with some added advantages:

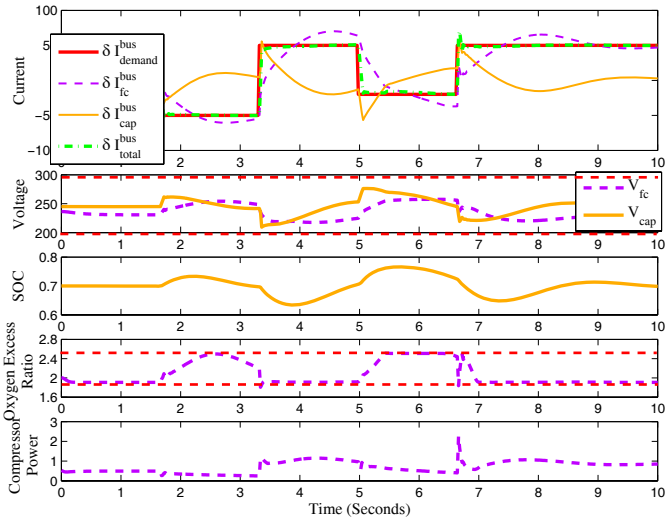

Fig. 8. Time response of the closed-loop fuel cell and ultracapacitor systems during step changes in current demand. The operator δ denotes current deviations from nominal. The horizontal dashed lines represent the constraints.

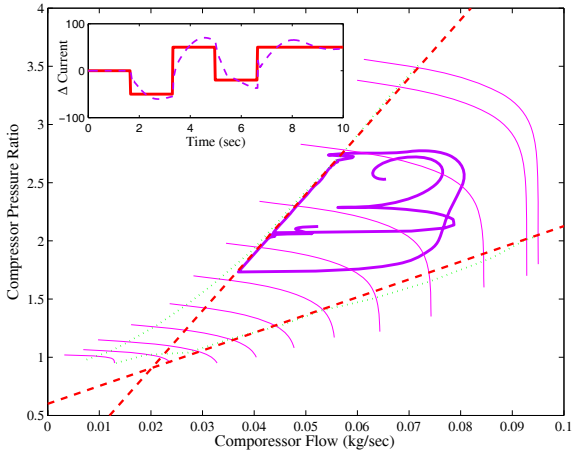

Fig. 9. Compressor map trajectory during fuel cell current transients shown in Fig. 8 and also shown in the insert plot.

1) The modular decentralized design, allows to run the two controllers on two different processors if needed, 2) each optimization problem is smaller, 3) unlike a centralized design and as shown in the simulations here, the prediction horizon used for the fuel cell controller can be different from that of the ultracapacitor controller 4) If needed and depending on the speed of each subsystem, different sampling times can be used for each controller.

V. Conclusions

We demonstrated that coordination of multiple power sources in a hybrid electric powertrain could be achieved by lower level decentralized MPCs which enforce the constraints and a simple rule-based supervisory scheme which coordinates the closed-loop subsystems. The concept is applied to a fuel cell-ultracapacitor hybrid for which we demonstrate a decentralized MPC can meet the system level power request while enforcing all the subsystem level constraints. The advantage over a centralized control scheme is reduced computations and more importantly compatibility with a modular powertrain architecture. We believe it is now time to consider decentralization in powertrain control applications as the complexity of modern powertrains is increasing and at the same time there are multiple processors onboard a vehicle that can share the computational load. Dedicated controllers for each subsystem which impose operational bounds in the form of pointwise-in-time constraints could help realize a "plug-and-play" powertrain in which subsystems provided by various suppliers can more easily and with minimal calibration be integrated in the powertrain.

VI. Acknowledgements

The first author would like to thank Dr. Ilya Kolmanovsky from Ford Motor Company's Research and Advanced Engineering for the initial discussion at the 2006 American Control Conference which led to this work.

References

[1] C.-C. Lin, H. Peng, J.-M. Kang, and J. Grizzle, "Power management strategy for a parallel hybrid electric truck," *IEEE Transactions on Control Systems Technology*, vol. 11, no. 6, pp. 839–849, 2003.

[2] P. Rodatz, G. Paganelli, A. Sciarretta, and L. Guzzella, "Optimal power management of an experimental fuel cell supercapacitor-powered hybrid vehicle," *Control Engineering Practice*, vol. 13, pp. 41–53, 2005.

[3] A. Vahidi, A. Stefanopoulou, and H. Peng, "Current management in a hybrid fuel cell power system: A model predictive control approach," *IEEE Transactions on Control Systems Technology*, vol. 14, pp. 1047–1057, 2006.

[4] E. Camponogara, D. Jia, B.H. Krogh, and S. Talukdar, "Distributed model predictive control," *IEEE Control Systems Magazine*, vol. 2, pp. 44–52, 2002.

[5] A. Richards and J. How, "Decentralized model predictive control of cooperating UAVs," *Proceedings of IEEE Conference on Decision and Control*, vol. 4, pp. 4286–4291, 2004.

[6] T. Keviczky, F. Borrelli, and G.J. Balas, "Stability analysis of decentralized RHC for decoupled systems," *Proceedings of 44th IEEE Conf. on Decision and Control*, December 2005.

[7] L. Magni and R. Scattolini, "Stabilizing decentralized model predictive control of nonlinear systems," *Automatica*, vol. 42, pp. 1231–1236, 2006.

[8] J. Pukrushpan, A. Stefanopoulou, and H. Peng, *Control of Fuel Cell Power Systems: Principles, Modeling, Analysis, and Feedback Design*, Springer-Verlag, London, UK, 2004.

[9] A. Vahidi, I. Kolmanovsky, and A. Stefanopoulou, "Constraint handling in a fuel cell system: A fast reference governor approach," *IEEE Transactions on Control Systems Technology*, vol. 15, pp. 86–98, 2007.

[10] Kyung-Won Suh and Anna Stefanopoulou, "Coordination of converter and fuel cell controllers," *International Journal of Energy Research*, vol. 29, pp. 1167–1189, 2005.

[11] G. Pannocchia and J. Rawlings, "Disturbance models for offset-free model-predictive control," *AIChE Journal*, vol. 49, no. 2, pp. 426–437, 2003.

[12] K. Muske and T. Badgwell, "Disturbance modeling for offset-free linear model predictive control," *Journal of Process Control*, vol. 12, pp. 617–632, 2002.

[13] J. Larminie and J. Lowry, *Electric Vehicle Technology Explained*, John Wiley and Sons, LTD, West Sussex, England, 2003.

[14] P. Rodatz, O. Garcia, L. Guzzella, F. Buchi, M. Bartschi, A. Tsukada, P. Dietrich, R. Kotz, G. Scherer, and A. Wokaun, "Performance and operational characteristics of a hybrid vehicle powered by fuel cells and supercapacitors," *SAE Paper 2003-01- 0418*, 2003.